Chapter 5

Longitudinal Structure Function F_L and DIS Cross Section Ratio $R = \frac{\sigma_L}{\sigma_T}$ at Small-x from Regge Behaviour of Gluon Distribution Function

In this chapter, the behaviour of gluon dominated longitudinal structure function F_L^g with respect to Bjorken variable x and Q^2 , the squared four-momentum transfer between lepton and nucleon in next-next-to-leading order (NNLO) at small-x is presented using the Regge like behaviour of the gluon distribution function. Here we have calculated t- and x-evolutions of the F_L^g structure function using the gluon distribution function obtained as a result of solution of the DGLAP evolution equation at small-x. We have also studied the behaviour of the DIS cross section ratio $R = \frac{\sigma_L}{\sigma_T}$ in this kinematical region. The calculated results are compared with recent H1 [1–5], ZEUS [6] data and DL [7] model results. We have also compared our results with the theoretical results predicted by MSTW08 [8], CT10 [9,10], ABM11 [11] and NNPDF2.3 [12,13] parameterizations. The results obtained can be explained within the framework of pQCD i.e., the evolution of structure function F_L^g increases towards low values of x. And the behaviour of F_L^g structure function shows resemblance with the gluon distribution function as it is originated from gluon distribution function. Contrary to it, the behaviour of the ratio R shows constant behaviour with respect to x and fixed Q^2 i.e., its behaviour is independent of the behaviour of gluon distribution function. A comparative analysis of our x-evolution results with the results obtained in chapter 4 is also studied here

which indicate that the behaviour of structure function can be studied using both the Regge behaviour of gluon distribution function and Taylor expansion method.

5.1 Theory

In pQCD, the Altarelli-Martinelli equation for longitudinal structure function $F_L(x, Q^2)$ of proton in terms of co-efficient function is given by [14, 15]

$$x^{-1}F_L = C_{L,ns} \otimes q_{ns} + < e^2 > (C_{L,s} \otimes q_s + C_{L,g} \otimes g). \tag{5.1}$$

Here q_{ns}, q_s and g are the flavour non singlet, flavour singlet and gluon distribution function, $< e^2 >= \frac{5}{18}$ is the average squared charge for even N_f (number of active light flavours) and the symbol $\otimes$ represents the standard Mellin convolution. $C_{L,a}(a = ns, s, g)$'s represent the co-efficient functions as described in chapter 4.

At small values of x ($x \leq 10^{-3}$) the gluon contribution to the F_L structure function dominates over the flavour singlet and non-singlet contribution [16]. Now the Altarelli-Martinelli equation for gluon dominating F_L structure function is given by

$$F_L^g(x, Q^2) = \int_x^1 \frac{dw}{w} C_{L,g}(w, Q^2) G\Big(\frac{x}{w}, Q^2\Big). \tag{5.2}$$

Here $C_{L,g}(w, Q^2)$ is the gluon co-efficient function for F_L known perturbatively up to first few orders in running coupling constant $\alpha_s(Q^2)$ [17] and can be written as

$$C_{L,g}(w, Q^2) = \frac{\alpha_s(Q^2)}{4\pi} C_{L,g}^1(w) + \Big(\frac{\alpha_s(Q^2)}{4\pi}\Big)^2 C_{L,g}^2(w) + \Big(\frac{\alpha_s(Q^2)}{4\pi}\Big)^3 C_{L,g}^3(w), \tag{5.3}$$

where $C_{L,g}^1(w)$, $C_{L,g}^2(w)$ and $C_{L,g}^3(w)$ are the gluon co-efficient function for F_L in LO, NLO and NNLO respectively [15]. The required LO, NLO and NNLO approximation of the gluon co-efficient functions for F_L [15, 18, 19] are defined in Appendix A.

Using the gluon co-efficient functions and the equation (5.2), we can calculate the F_L^g structure function up to NNLO approximation. For this purpose, we have to first

determine the gluon distribution function $G(x,Q^2)$. We calculate this by solving the DGLAP evolution equation for gluon distribution function at small-x using the Regge like behaviour of the gluon distribution function. At small values of x, neglecting the quark singlet part, the DGLAP evolution equation for gluon distribution function is given by [20]

$$Q^2\frac{\partial G(x,Q^2)}{\partial Q^2} = \int_x^1 \frac{dw}{w} P_{gg}(w,Q^2) G\Big(\frac{x}{w},Q^2\Big). \tag{5.4}$$

Here $P_{gg}(w,Q^2)$ is the gluon splitting function known perturbatively up to first few orders in running coupling constant $\alpha_s(Q^2)$ and can be written as

$$P_{gg}(w,Q^2) = \frac{\alpha_s(Q^2)}{2\pi}P^1_{gg}(w) + \Big(\frac{\alpha_s(Q^2)}{2\pi}\Big)^2 P^2_{gg}(w) + \Big(\frac{\alpha_s(Q^2)}{2\pi}\Big)^3 P^3_{gg}(w), \tag{5.5}$$

up to NNLO, where $P^1_{gg}(w)$, $P^2_{gg}(w)$ and $P^3_{gg}(w)$ are the gluon splitting functions [20–22] in LO, NLO and NNLO respectively. At small-x limit the expressions for these splitting functions are defined in Appendix A.

Using the expressions for gluon splitting functions in equation (5.4) and simplifying the DGLAP evolution equations for the gluon distribution function $G(x,Q^2)$ in LO, NLO and NNLO, we get

$$\frac{\partial G(x,t)}{\partial t} = \frac{\alpha_s(t)}{2\pi}\Big[6\Big\{\Big(\frac{11}{12}-\frac{N_f}{18}\Big) + ln(1-x)\Big\}G(x,t) + 6I^1_g(x,t)\Big], \tag{5.6}$$

$$\begin{aligned}\frac{\partial G(x,t)}{\partial t} &= \frac{\alpha_s(t)}{2\pi}\Big[6\Big\{\Big(\frac{11}{12}-\frac{N_f}{18}\Big) + ln(1-x)\Big\}G(x,t) + 6I^1_g(x,t)\Big] \\ &\quad + \Big(\frac{\alpha_s(t)}{2\pi}\Big)^2 I^2_g(x,t),\end{aligned} \tag{5.7}$$

$$\begin{aligned}\frac{\partial G(x,t)}{\partial t} &= \frac{\alpha_s(t)}{2\pi}\Big[6\Big\{\Big(\frac{11}{12}-\frac{N_f}{18}\Big) + ln(1-x)\Big\}G(x,t) + 6I^1_g(x,t)\Big] \\ &\quad + \Big(\frac{\alpha_s(t)}{2\pi}\Big)^2 I^2_g(x,t) + \Big(\frac{\alpha_s(t)}{2\pi}\Big)^3 I^3_g(x,t),\end{aligned} \tag{5.8}$$

where

$$I_g^1(x,t) = \int_x^1 dw \left[\frac{wG\left(\frac{x}{w},t\right) - G(x,t)}{(1-w)} + \left\{ w(1-w) + \frac{1-w}{w} \right\} G\left(\frac{x}{w},t\right) \right], \tag{5.9}$$

$$I_g^2(x,t) = \int_x^1 dw P_{gg}^2(w) G\left(\frac{x}{w},t\right) \tag{5.10}$$

and

$$I_g^3(x,t) = \int_x^1 dw P_{gg}^3(w) G\left(\frac{x}{w},t\right). \tag{5.11}$$

Now, the Regge like behaviour of the gluon distribution function can be expressed as [23]

$$G(x,t) = f(t) x^{-\lambda_g}, \tag{5.12}$$

where $f(t)$ is a function of t and t is defined in chapter 2, and λ_g is the Regge exponent. Now, $G\left(\frac{x}{w},t\right)$ can be written as

$$G\left(\frac{x}{w},t\right) = G(x,t) w^{\lambda_g}. \tag{5.13}$$

Using equations (5.12) and (5.13) in equation (5.6) we get

$$\frac{\partial G(x,t)}{\partial t} = \frac{G(x,t)}{t} P(x), \tag{5.14}$$

where

$$\begin{aligned} P(x) &= \frac{12}{\beta_0} \left[\left(\frac{11}{12} - \frac{N_f}{18} \right) + ln(1-x) \right. \\ &\quad \left. + \int_x^1 dw \left\{ \frac{w^{1+\lambda_g} - 1}{1-w} + w^{\lambda_g} \left(w(1-w) + \frac{1-w}{w} \right) \right\} \right]. \end{aligned} \tag{5.15}$$

Integrating equation (5.14) we get

$$G(x,t) = Ct^{P(x)}, \tag{5.16}$$

where C is a constant of integration and can be determined from experimental data.

Applying initial conditions at $t = t_0$, $G(x,t) = G(x,t_0)$ and at $x = x_0$, $G(x,t) = G(x_0,t)$, the t- and x-evolutions for $G(x,t)$ gluon distribution function in LO can be written as

$$G(x,t) = G(x,t_0)\Big(\frac{t}{t_0}\Big)^{P(x)} \tag{5.17}$$

and

$$G(x,t) = G(x_0,t)t^{[P(x)-P(x_0)]} \tag{5.18}$$

respectively.

Proceeding in the similar manner from equation (5.7)and (5.8), we obtain the t- and x-evolution equations for $G(x,t)$ gluon distribution function in NLO as

$$G(x,t) = G(x,t_0)\frac{t^{(1+\frac{b}{t})Q(x)}}{t_0^{(1+\frac{b}{t_0})Q(x)}} exp\Big[b\Big(\frac{1}{t}-\frac{1}{t_0}\Big)Q(x)\Big] \tag{5.19}$$

and

$$G(x,t) = G(x_0,t)t^{(1+\frac{b}{t})[Q(x)-Q(x_0)]} exp\Big[\frac{b}{t}(Q(x)-Q(x_0))\Big] \tag{5.20}$$

respectively, and in NNLO as

$$G(x,t) = G(x,t_0)\frac{t^{(1+b/t)S(x)}}{t_0^{(1+b/t_0)S(x)}} \exp\left[\begin{array}{c} \Big\{b\Big(\frac{1}{t}-\frac{1}{t_0}\Big)+\Big(\frac{b^2}{2}-\frac{c}{2}\Big)\Big(\frac{1}{t^2}-\frac{1}{t_0^2}\Big) \\ -\frac{b^2}{2}\Big(\frac{ln^2 t}{t^2}-\frac{ln^2 t_0}{t_0^2}\Big)\Big\}S(x) \end{array}\right] \tag{5.21}$$

and

$$G(x,t) = G(x_0,t)t^{(1+b/t)\{S(x)-S(x_0)\}} \cdot \exp\left[\begin{array}{c}\left\{\frac{b}{t}+\left(\frac{b^2}{2}-\frac{c}{2}\right)\left(\frac{1}{t^2}\right)-\frac{b^2}{2}\left(\frac{ln^2t}{t^2}\right)\right\}\\ \{S(x)-S(x_0)\}\end{array}\right] \quad (5.22)$$

respectively. Here

$$Q(x) = [P(x) + T_0R(x)], \qquad R(x) = -27.11\frac{1-x^{\lambda_g}}{\lambda_g} + 98.9\Big(\frac{1-x^{1+\lambda_g}}{1+\lambda_g}\Big),$$

$$S(x) = [P(x) + T_0R(x) + T_1Y(x)], \qquad \text{and} \qquad Y(x) = -149.33\frac{(1-x^{\lambda_g-1})}{\lambda_g-1}.$$

The numerical parameters T_0 and T_1 are calculated from the data as described in chapter 2 and ref. [24]. Here $T_0 = 0.0278$ and $T_1 = 0.00013$ in our required Q^2 range $1.5 \leq Q^2 \leq 800GeV^2$.

Thus we have obtained an analytical expression for the t- and x-evolutions of gluon distribution function $G(x,t)$ in LO, NLO and NNLO. Using the above expressions of gluon distribution function along with the co-efficient functions we have calculated F_L^g structure functions in LO, NLO and NNLO.

In a similar manner, the F_2^g structure function can be determined at small-x with the help of the calculated results of gluon distribution function using the equation [25]

$$F_2^g(x,Q^2) =< e^2 > \int_x^1 dw C_{2,g}(w)G\Big(\frac{x}{w},Q^2\Big). \quad (5.23)$$

Here $C_{2,g}(w)$ is the gluon co-efficient function for F_2 and can be written as

$$C_{2,g}(w,Q^2) = \frac{\alpha_s(Q^2)}{4\pi}C^1_{2,g}(w) + \Big(\frac{\alpha_s(Q^2)}{4\pi}\Big)^2 C^2_{2,g}(w) + \Big(\frac{\alpha_s(Q^2)}{4\pi}\Big)^3 C^3_{2,g}(w) \quad (5.24)$$

up to NNLO, where $C^1_{2,g}(w)$, $C^2_{2,g}(w)$ and $C^3_{2,g}(w)$ are the gluon co-efficient functions [26] for F_2 structure function in LO, NLO and NNLO respectively and are defined in Appendix A.

The measurements of longitudinal structure function F_L are used to determine the DIS cross section ratio R which is related to the structure functions F_2 and F_L as

$$R = \frac{\sigma_L}{\sigma_T} = \frac{F_L}{F_2 - F_L}, \tag{5.25}$$

where σ_L and σ_T are the absorption cross sections of longitudinally and transversely polarized virtual photons by proton. At small-x, F_2 and F_L are gluon dominating and so equation (5.25) can be written as

$$R = \frac{F_L^g}{F_2^g - F_L^g}. \tag{5.26}$$

In analogy with the F_L structure function the ratio R is a good QCD characteristic because it equals zero in the naive parton model. Moreover at small values of x, the ratio R gives the relative strength of the two components of the absorption cross section [6, 27]. Here, we have also studied the behaviour of ratio R at small-x in LO, NLO and NNLO using the calculated values of F_L^g and F_2^g structure function.

5.2 Results and Discussions

We have calculated the t- and x-evolutions of the gluon dominating longitudinal proton structure function F_L at small-x up to next-next-to-leading order approximation using the gluon distribution function. This gluon distribution function is obtained as a result of solution of the DGLAP evolution equation for gluon distribution at small-x. To extract the gluon density inside proton, we use Regge like behaviour of the gluon distribution function. For this purpose, we use the input distribution of gluon from DL model [7], MSTW08 [8], CT10 [9, 10], ABM11 [11] and NNPDF2.3 [12, 13] to obtain t- and x-evolutions of the gluon density. As the values of Regge exponent is close to 0.5 in the region of small-x [28], we have taken its value as 0.5. Thus using the required co-efficient function which are given in Appendix A and gluon distribution

function we have calculated the F_L^g structure function in the range $10^{-4} \leq x \leq 0.1$ and $1.5 \leq Q^2 \leq 800GeV^2$.

The obtained results are compared with the available H1 [1–5], ZEUS [6] experimental data and results of DL model fit [7], MSTW08 [8], CT10 [9, 10], ABM11 [11] and NNPDF2.3 [12, 13] parameterizations. The related plots are shown in figures 5.1 to 5.6 which indicate a good agreement with the experimental data, related fit and parameterizations. In all the graphs, the lowest-Q^2 and highest-x points are taken as input for $G(x, t_0)$ and $G(x_0, t)$ respectively. Here, the vertical error bars are both statistical and systematic errors for both H1 and ZEUS data. To confirm that in spite of the large uncertainty in the experimental data, our results are in good agreement with the data, we add DL model results and the theoretical prediction of different parameterizations in all the figures. Figure 5.1 represents the t-evolution results of F_L^g structure function which show that our results are compatible with the data and the results of DL model. Here the structure function increases with the increase of Q^2. The x-evolution results are depicted in figure 5.2 to 5.6 which reflect better agreement of our results with data and results of the model and parameterizations. These graphs describe that the behaviour of structure function F_L^g increases towards small values of x. In case of the x-evolution results described in figure 5.2 to figure 5.6, the behaviour of LO, NLO curves are not exactly the same as we have considered the input point from different parameterizations. In all the graphs it is observed that our results show good agreement with data, related model fit and parameterizations as the energy scale becomes larger. It is observed from the t- and x-evolutions results that the behaviour of the LO, NLO and NNLO curves are different in both the cases. Thee reason for this is that the expressions for the calculation of t- and x-evolutions are different and the behaviour of LO, NLO, NNLO curves depends on the expressions only. Moreover, with reference to some recent papers [29–32], we can say that the pattern of LO, NLO, NNLO curves (i.e., sometimes NLO results overestimate LO prediction and vice versa)

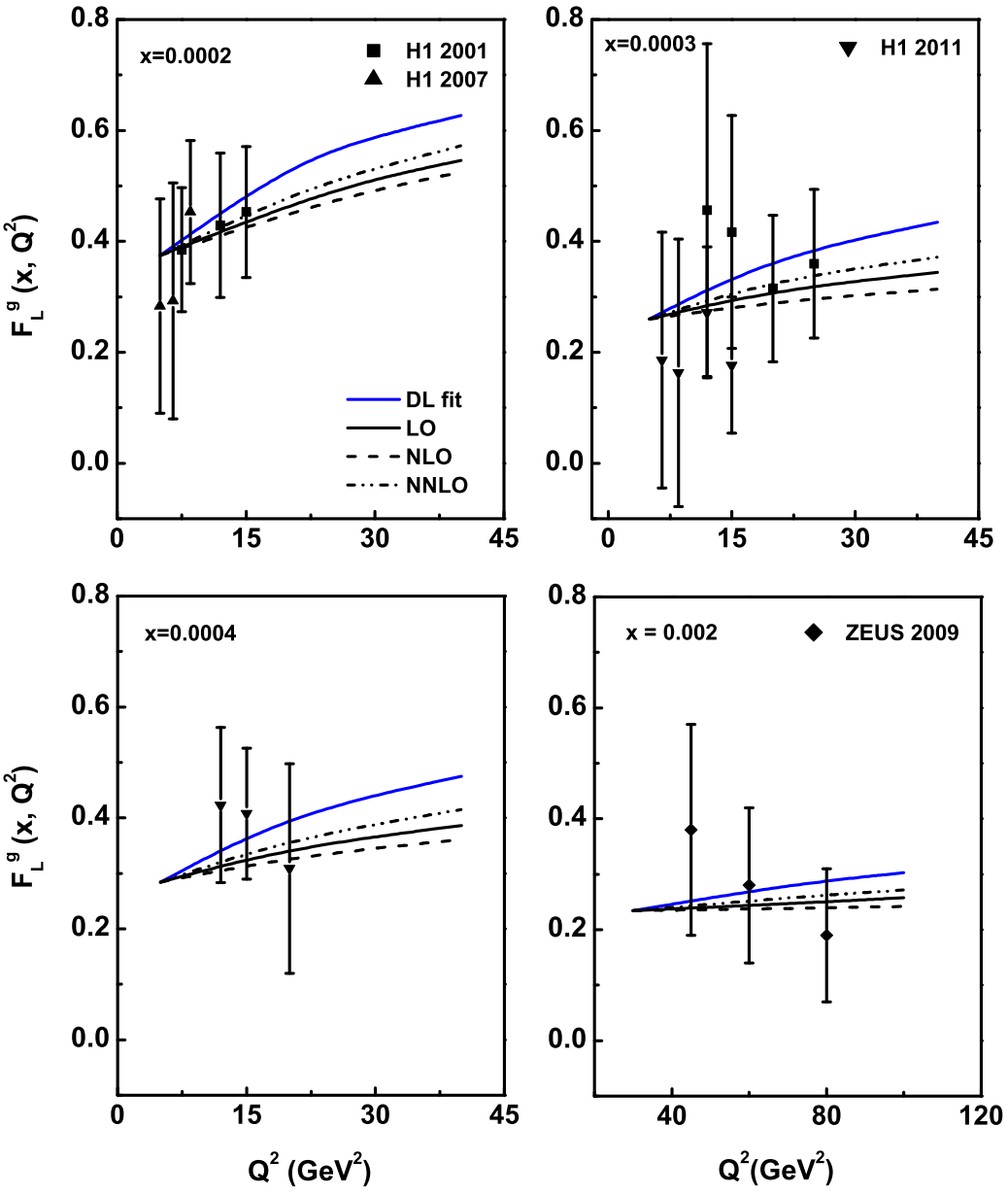

Figure 5.1: t-evolution results of F_L^g structure function up to NNLO using Regge theory in comparison with the H1, ZEUS data and results of DL model.

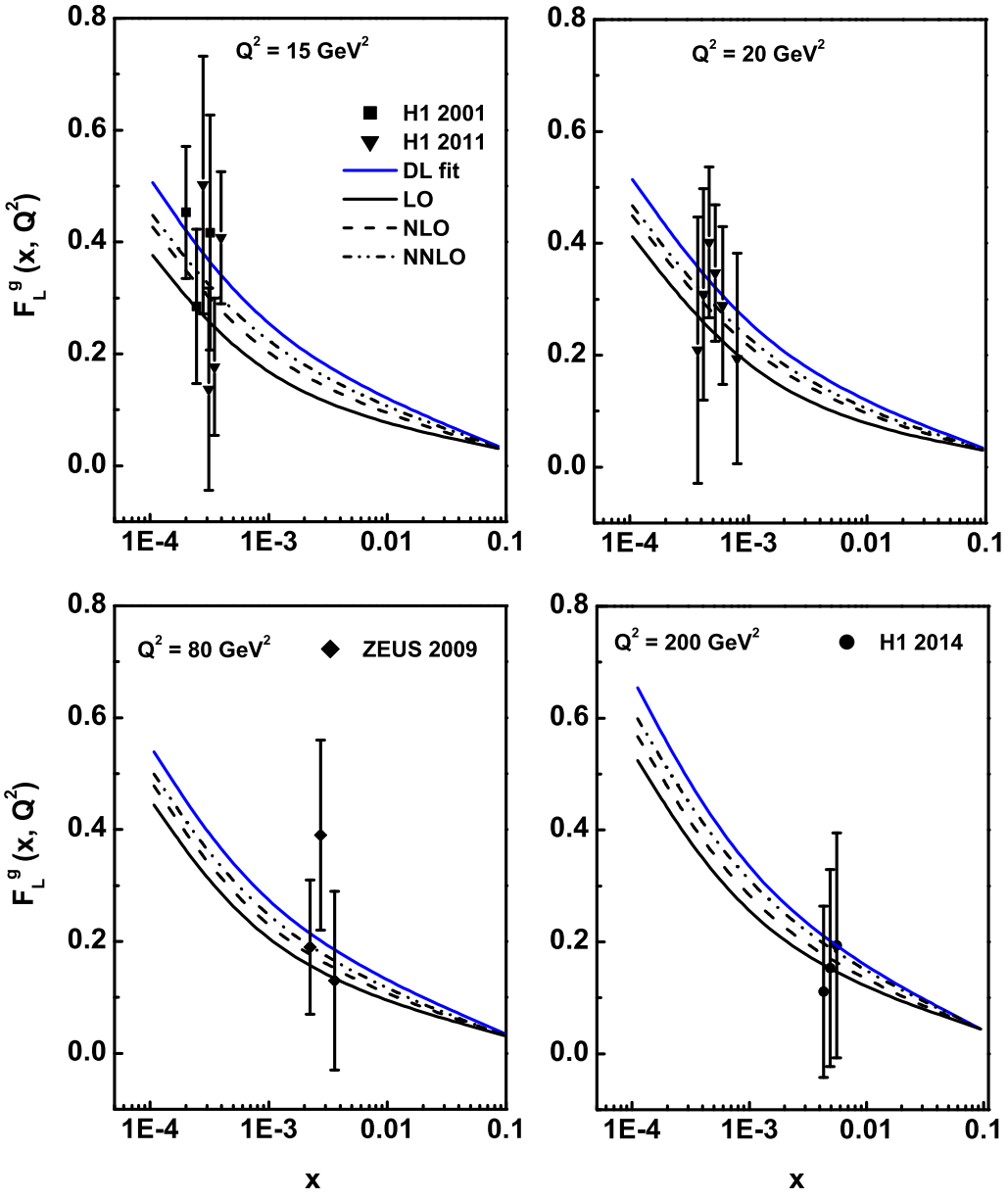

Figure 5.2: x-evolution results of F_L^g structure function up to NNLO using Regge theory in comparison with the H1, ZEUS data and results of DL model.

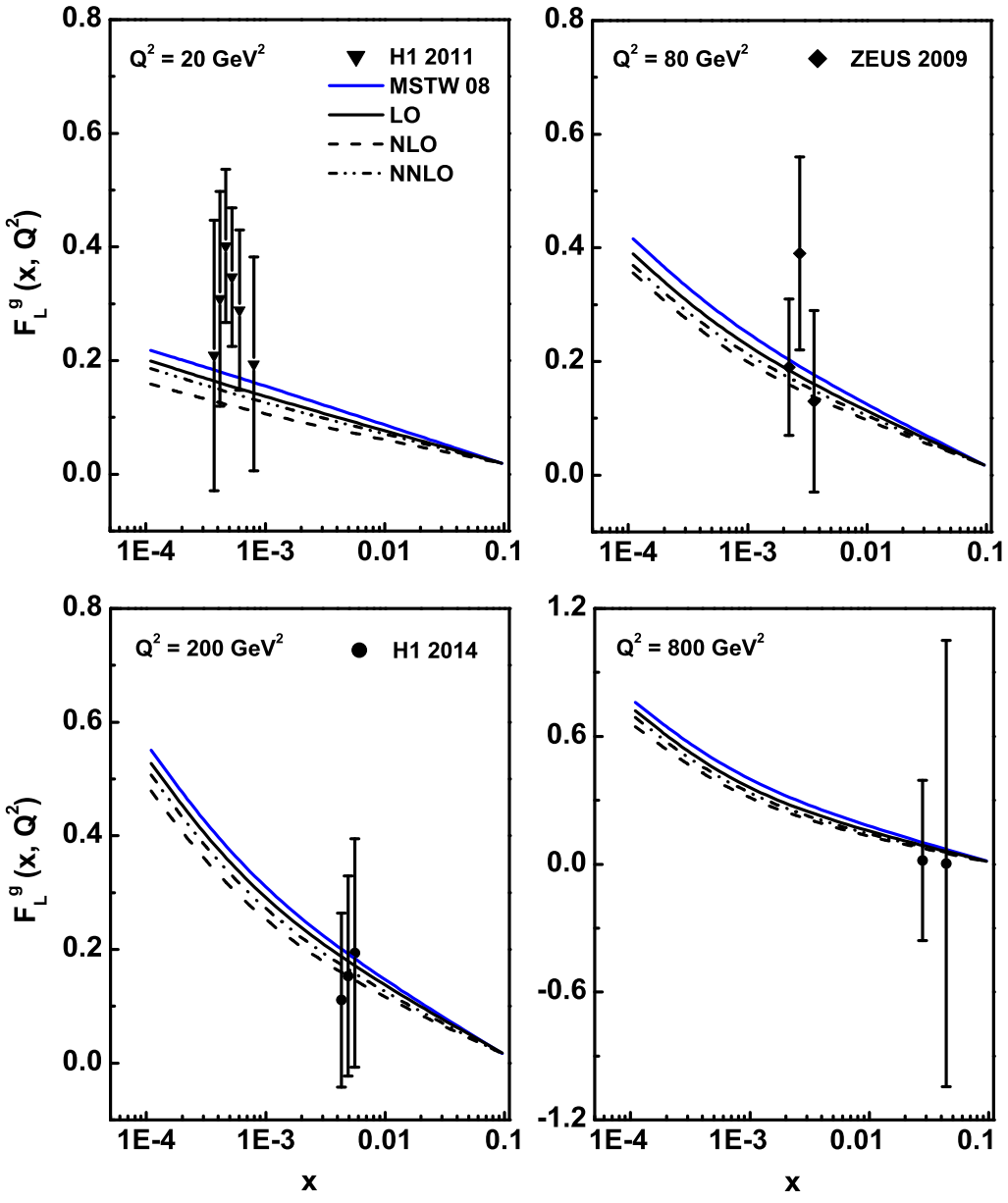

Figure 5.3: x-evolution results of F_L^g structure function up to NNLO using Regge theory in comparison with the H1, ZEUS data and the theoretical prediction of MSTW08.

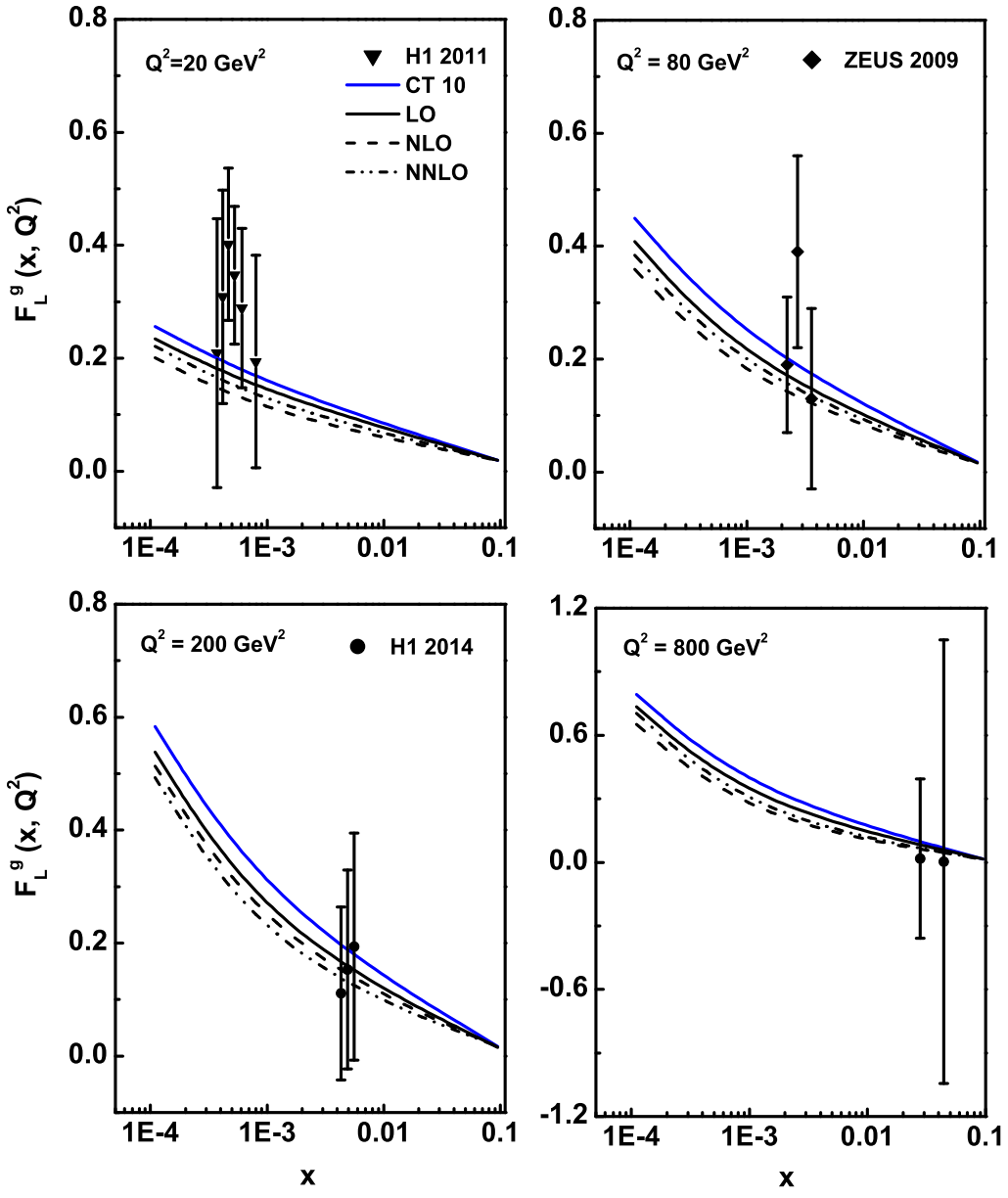

Figure 5.4: x-evolution results of F_L^g structure function up to NNLO using Regge theory in comparison with the H1, ZEUS data and the theoretical prediction of CT10.

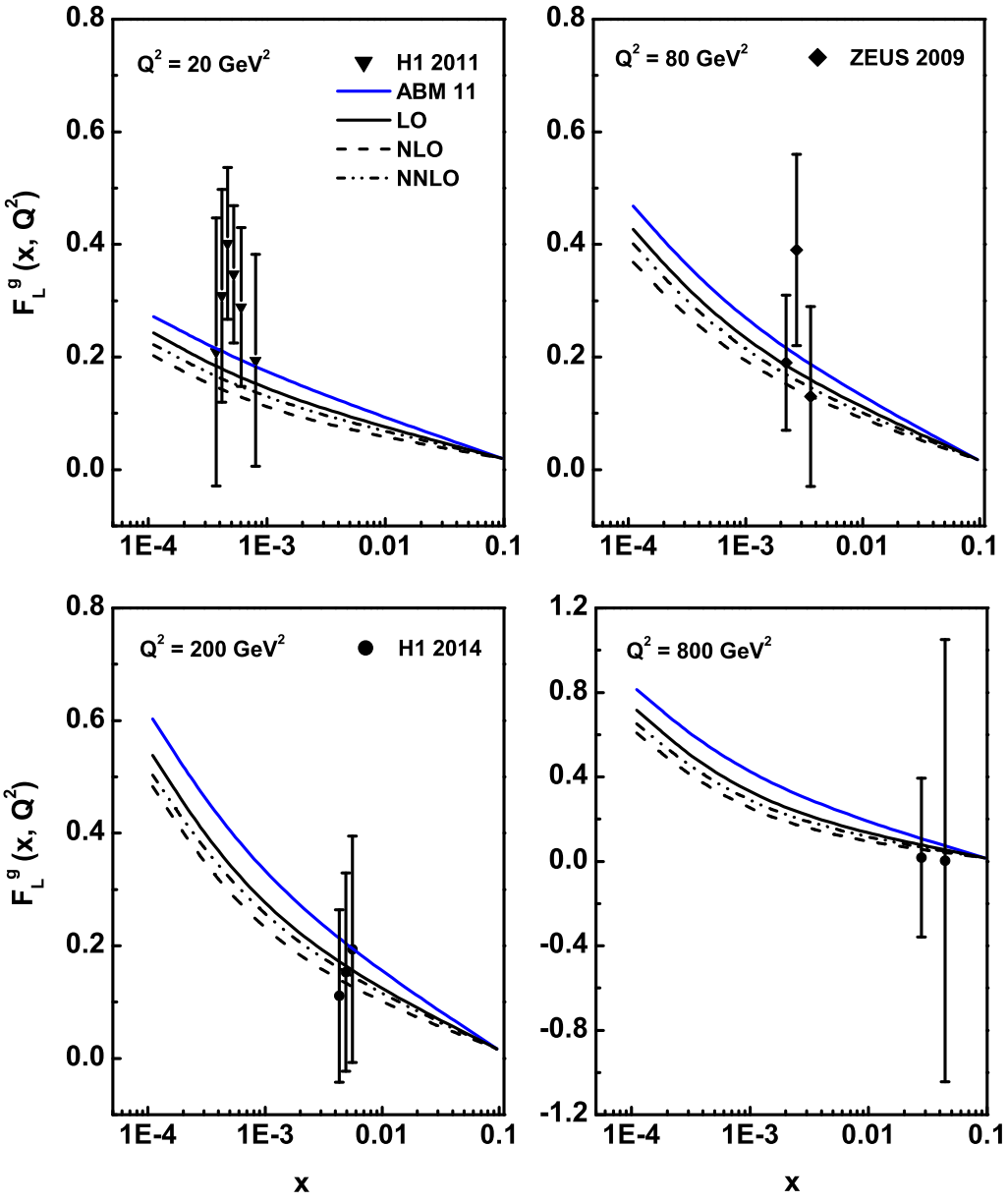

Figure 5.5: x-evolution results of F_L^g structure function up to NNLO using Regge theory in comparison with the H1, ZEUS data and the theoretical prediction of ABM11.

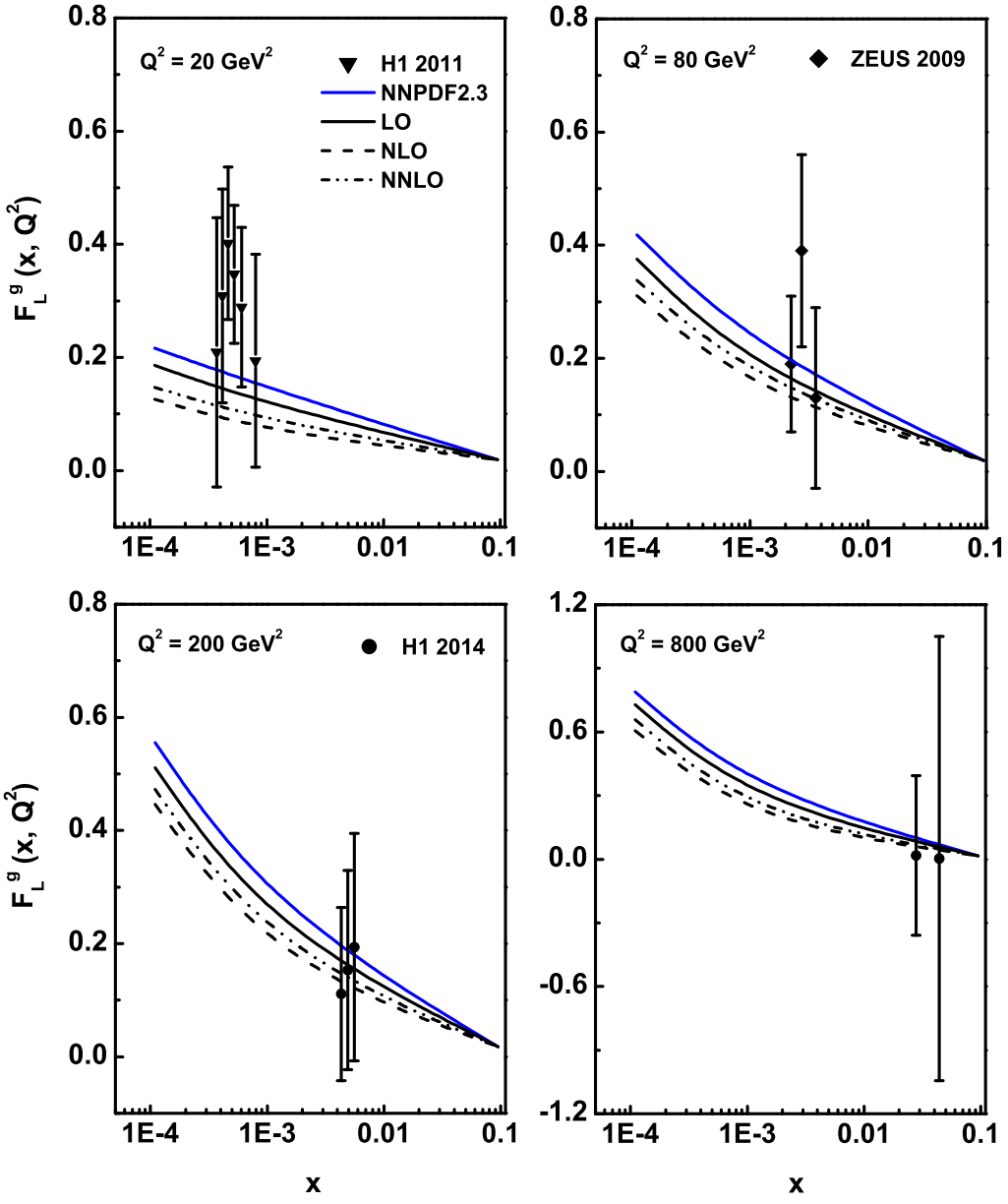

Figure 5.6: x-evolution results of F_L^g structure function up to NNLO using Regge theory in comparison with the H1, ZEUS data and the theoretical prediction of NNPDF2.3.

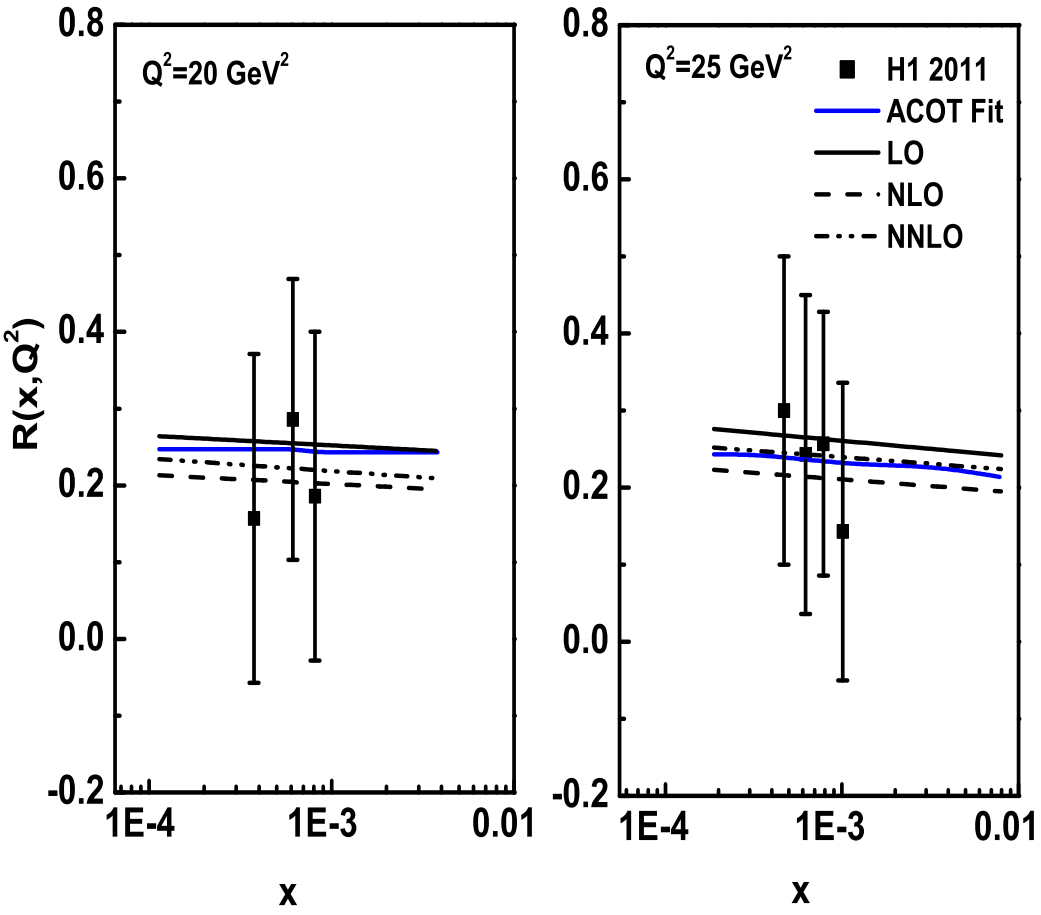

Figure 5.7: x-evolution results of R in comparison with the H1 data and the theoretical prediction of ACOT fit.

depend only on the applied method.

We have also calculated the cross section ratio R using the results of the F_2^g and F_L^g structure functions from equations (5.2) and (5.23). In figure 5.7, the ratio R is plotted against x for different values of Q^2 in comparison with the H1 data and the prediction of DGLAP fit in the ACOT scheme [33]. ACOT scheme incorporates the heavy quark mass into the theoretical calculations of massive partonic cross section.

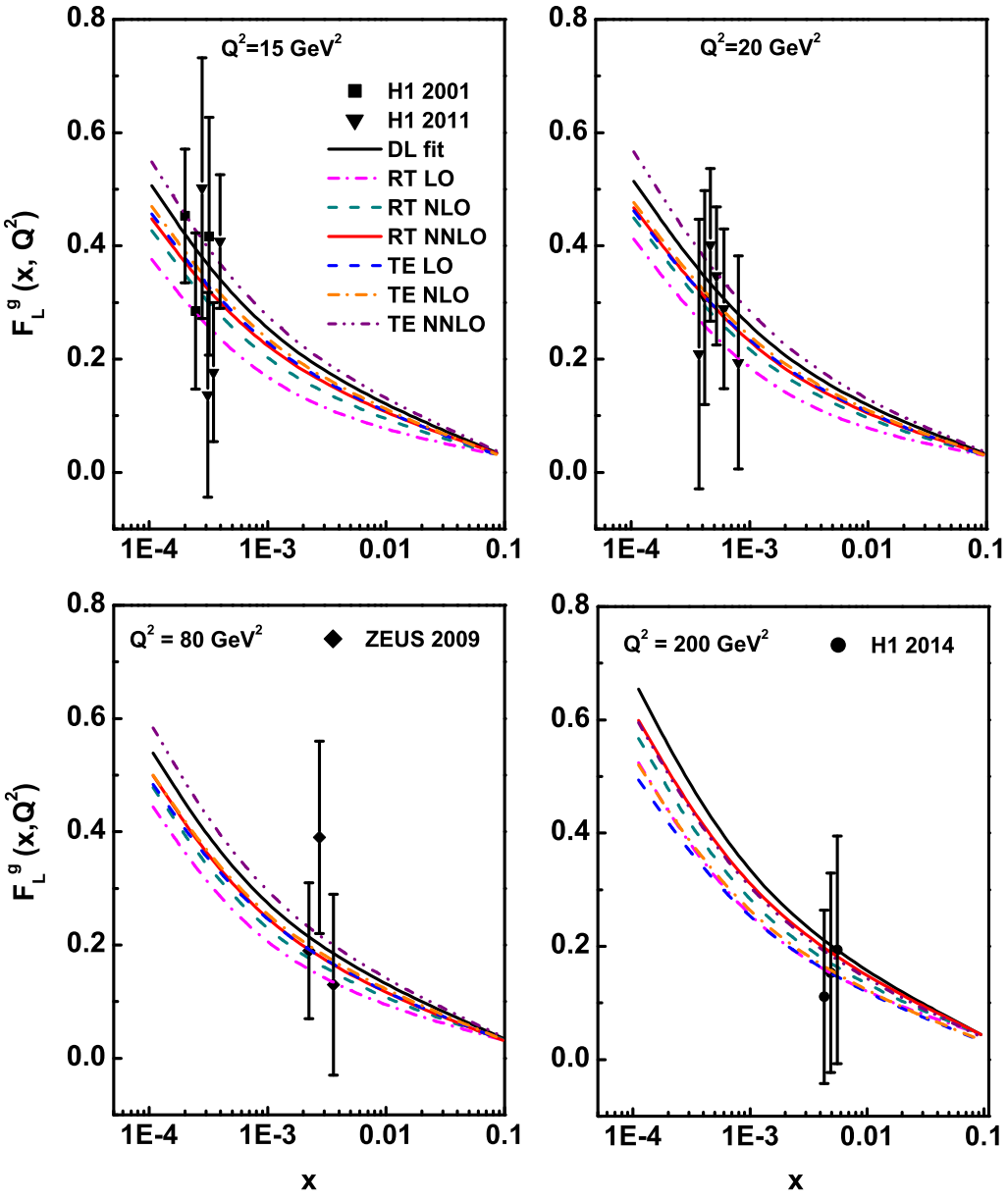

Figure 5.8: Comparison of x-evolution results of F_L^g structure function up to NNLO using Regge theory (RT) and Taylor expansion (TE) method in comparison with the H1, ZEUS data and the of DL model.

Here they have used the QCDNUM program [34] for the DGLAP evolution which helps to generate the PDFs from an initial distribution based on the Les Houches benchmark set [35]. Together with the precise HERA data, these calculations facilitate accurate determination of PDFs. We have analyzed the behaviour of the ratio R for two values of $Q^2 = 20GeV^2, 25GeV^2$ which indicate good agreement with the experimental data and fit. It has been observed in the H1 experimental results that for $Q^2 \geq 3.5GeV2$, the ratio R is consistent with a constant behaviour [1]. Our analysis also shows constant behavior with respect to x for fixed values of Q^2. The constant behaviour of the cross section ratio implies that its behaviour is independent of the behaviour of gluon distribution function with respect to x at small-x.

5.2.1 Comparative study of our results obtained by Regge theory and Taylor expansion method

We have also presented a comparison of our x-evolution results and the results obtained in the chapter 4 which is shown in figure 5.8. These two results are actually the results of F_L^g structure function obtained by Regge theory (RT) and Taylor expansion (TE) method. The comparison of the results of F_L structure function obtained in both the cases shows similar behaviour with the model fit and data. Thus one can determine the evolution of structure function using both the methods.

5.3 Conclusions

In this chapter, we have calculated the gluon dominating longitudinal structure function F_L^g of proton up to NNLO approximation from DGLAP evolution equation for gluon distribution function at small-x using the Regge like behaviour of the gluon distribution function. The evolutions of F_L structure function with x and Q^2 reflects similar nature with the experimental data which shows the compatibility of Regge behaviour with the perturbative evolution of structure function at small-x. To confirm the validity of our

calculations we compare our results with the recent experimental data taken by H1 and ZEUS collaborations along with the DL model results and the theoretical prediction of different parameterizations. Our results are in good agreement with the data and related fits. As in our given range of x, the gluon contribution to the structure function is dominant one, so we can conclude in general that the gluon contribution to the longitudinal structure function increases with the decreasing values of x. We have also calculated the cross section ratio R which indicates good agreement with the H1 data and DGLAP fit in the ACOT scheme. Its variation with small values of Bjorken variable x and fixed Q^2 shows constant behaviour similar to that of the experimental data and fit. From the constant behaviour of the cross section ratio R with respect to x, we can conclude that its behaviour does not depend on the behaviour of gluon distribution function with respect to x and fixed Q^2 at small-x. The comparative analysis of our x-evolution results with that of the results obtained in chapter 4 show good agreement with data and the related model fit. In chapter 4, Taylor expansion method is used to evaluate the structure function. Thus, we can conclude that both Regge theory and Taylor expansion method can be used to study the behaviour of the structure function in small-x region.

References

[1] Aaron, F. D., et al. Measurement of the inclusive $e^{\pm}p$ scattering cross section at high inelasticity y and of the structure function F_L, *Eur. Phys. J. C.* **71** (3), 1579-1–50, 2011.

[2] Adloff, C., et al. Deep-inelastic inclusive ep scattering at low x and a determination of α_s, *Eur. Phys. J. C.* **21** (1), 33–61, 2001.

[3] Pardos, C. D. *Studies for the direct measurement of the proton structure function F_L with the H1 detector at HERA*, Ph.D. thesis, DESY, Zeuthen, Germany, 2007.

[4] Piec, S. *Measurement of the Proton Structure Function F_L with the H1 Detector at HERA*, Ph.D. thesis, Humboldt University of Berlin, Germany, 2009.

[5] Andreev, V., et al. Measurement of Inclusive *ep* Cross Sections at High Q^2 at $\sqrt{s} = 225$ and $252GeV$ and of the Longitudinal Proton Structure Function F_L at HERA, *Eur. Phys. J. C* **74** (4), 2814-1–26, 2014.

[6] Chekanov, S., et al. Measurement of the longitudinal proton structure function at HERA, *Phys. Lett. B* **682** (1), 8–22, 2009.

[7] Donnachie, A. and Landshoff, P. V. The protons gluon distribution, *Phys. Lett. B* **550** (3-4), 160–165, 2002.

[8] Martin, A. D., et al. Parton distributions for the LHC, *Eur. Phys. J. C* **63** (2), 189–285, 2009.

[9] Hung-Liang, Lai., et al. New parton distributions for collider physics, *Phys. Rev. D* **82** (7), 074024-1–24, 2010.

[10] Jun, Gao., et al. CT10 next-to-next-to-leading order global analysis of QCD, *Phys. Rev. D* **89** (3), 033009-1–28, 2014.

[11] Alekhin, S., Bluemlein, J. and Moch, S. The ABM parton distributions tuned to LHC data, *Phys. Rev. D* **89** (5), 054028-1–21, 2014.

[12] Ball, R. D., et al. Parton distributions with LHC data, *Nucl. Phys. B* **867** (2), 244–289, 2013.

[13] Forte, S., et al. Heavy quarks in deep-inelastic scattering, *Nucl. Phys. B* **834** (1-2), 116–162, 2010.

[14] Altarelli, G. and Martinelli, G. Transverse momentum of jets in electroproduction from quantum chromodynamics, *Phys. Lett. B* **76** (1), 89–94, 1978.

[15] Moch, S., Vermaseren, J. A. M. and Vogt, A. The longitudinal structure function at the third order, *Phys. Lett. B* **606** (1-2), 123–129, 2005.

[16] Cooper-Sarkar, A. M., et al. Measurement of the longitudinal structure function and the small x gluon density of the proton, *Z. Phys. C* **39** (2), 281–290, 1988.

[17] Abbott, L. F., Atwood, W. B. and Barnett, R. M. Quantum-chromodynamic analysis of eN deep-inelastic scattering data, *Phys. Rev. D* **22** (3), 582–593, 1980.

[18] Zijlstra, E. B. and Van Neerven, W. L. Contribution of the second order gluonic Wilson coefficient to the deep inelastic structure function, *Phys. Lett. B* **273** (4), 476–482, 1991.

[19] Moch, S. and Vermaseren, J. A. M. Deep-inelastic structure functions at two loops, *Nucl. Phys. B* **573** (3), 853–907, 2000.

[20] Furmanski, W. and Petronzio, R. Singlet parton densities beyond leading order, *Phys. Lett. B* **97** (3-4), 437–442, 1980.

[21] Altarelli, G. and Parisi, G. Asymptotic freedom in parton language, *Nucl. Phys. B* **126** (2), 298–318, 1977.

[22] Ellis, R. K., Kunszt, Z. and Levin, E. M. The evolution of parton distributions at small x, *Nucl. Phys. B* **420** (3), 517–549, 1994.

[23] Kotikov, A. V. and Parente, G. The gluon distribution as a function of F_2 and $dF_2/dlnQ^2$ at small x. The next-to-leading analysis, *Phys. Lett. B* **379** (1-4), 195–201, 1996.

[24] Baishya, R. and Sarma, J. K. Semi numerical solution of non-singlet DokshitzerGribovLipatovAltarelliParisi evolution equation up to next-to-next-to-leading order at small x, *Eur. Phys. J. C* **60** (4), 585–591, 2009.

[25] Vermaseren, J. A. M., Vogt, A. and Moch, S. The third-order QCD corrections to deep-inelastic scattering by photon exchange, *Nucl. Phys. B* **724** (1-2), 3–182, 2005.

[26] Neerven, W. L. Van and Vogt, A. NNLO evolution of deep-inelastic structure functions: the singlet case, *Nucl. Phys. B* **588** (1-2), 345–373, 2000.

[27] Aaron, F. D., et al. Combined measurement and QCD analysis of the inclusive e p scattering cross sections at HERA, *J. High Energy Phys.* **2010** (1), 109-1–63, 2010.

[28] Martin, A. D., Ryskin, M. G. and Watt, G. Simultaneous QCD analysis of diffractive and inclusive deep-inelastic scattering data, *Phys. Rev. D* **70** (9), 091502-1–5, 2004.

[29] Rezaei, B. and Boroun, G. R. Analytical solution of the longitudinal structure function F_L in the leading and next-to-leading-order analysis at low x with respect to Laguerre polynomials method, *Nucl. Phys. A* **857** (1), 42–47, 2011.

[30] Nematollahi, H., Yazdanpanah, M. M. and Mirjalili, A. NNLO longitudinal proton structure function, based on the modified χQM, *Mod. Phys. Lett. A* **27** (31),1250179-1-11 ,2012.

[31] Boroun, G. R. and Rezaei, B. Analysis of the proton longitudinal structure function from the gluon distribution function, *Eur. Phys. J. C* **72** (11), 2221-1-5, 2012.

[32] Devee, M., Baishya, R. and Sarma, J. K. Evolution of singlet structure functions from DGLAP equation at next-to-next-to-leading order at small-x, *Eur. Phys. J. C* **72** (6), 2036-1-11, 2012.

[33] Kramer, M., Olness, F. I. and Soper, D. E. Treatment of heavy quarks in deeply inelastic scattering, *Phys. Rev. D* **62** (9), 096007-1–9, 2000.

[34] Botje, M. QCDNUM: Fast QCD evolution and convolution, *Comput. Phys. Commun.* **182** (2), 490–532, 2011.

[35] Giele, W., et al. The QCD/SM Working Group: Summary Report, FERMILAB-Conf-02/410 (2004), arXiv:hep-ph/0204316. □